RSC Advances

PAPER

View Article Online
View Journal | View Issue

Cite this: *RSC Adv.*, 2014, **4**, 33446

Oxalate capped iron nanomaterial: from methylene blue degradation to bis(indolyl)methane synthesis†

Rupa Pegu, Krishna Joyti Majumdar, Dhruba Joyti Talukdar and Sanjay Pratihar*

An efficient, sustainable and green procedure for the synthesis of selective orthorhombic iron(oxalate) capped Fe(0) [Fe(ox)–Fe(0)] nanomaterial is developed using sodium borohydride ($NaBH_4$) reduction of iron(II) salt in the presence of oxalic acid at room temperature in water. The reported method is a cost-effective chemical route for producing Fe(ox)–Fe(0) nanomaterial on the gram scale without high-temperature calcination. The oxidation of Fe(0) to Fe_3O_4 at room temperature in open air leads to Fe-oxalate capped Fe_3O_4 [Fe(ox)–Fe_3O_4] nanomaterial on the gram scale. The Fe(ox)–Fe_3O_4 nanomaterial is found to be useful as a magnetically recoverable catalyst for the selective synthesis of bis(indolyl)methanes from the condensation between aldehydes and indoles in water. The as-prepared Fe(ox)–Fe_3O_4 nanomaterials also show an excellent ability as a reusable catalyst for the degradation of methylene blue (MB) under UV irradiation and are expected to be useful in many other applications. Aqueous reaction medium, easy synthesis, effortless separation of the catalyst using an external magnet, and efficient recycling of the catalyst make the protocol economical and sustainable.

Received 7th May 2014
Accepted 23rd July 2014

DOI: 10.1039/c4ra04214j

www.rsc.org/advances

Introduction

Amongst various nanoparticles (NPs), metallic magnetic nanoparticles (NPs) having different shapes and sizes have received considerable attention in the past decade because of their various applications.[1] In particular, iron oxide nanoparticles have been of great interest, not only in fundamental properties caused by their multivalent oxidation states, abundant polymorphism, and the mutual polymorphous changes in nanophase, but also in technological applications such as high density magnetic recording media, sensors, catalysts, and clinical usage. The enormous popularity of iron oxides as catalysts derives from their broad application potential due to easy handling, reasonably low cost, nontoxicity, and environmentally friendly character.[2] Currently, iron oxide catalysts are utilized on large scale in laboratory, industrial, and environmental processes to accelerate various reactions including oxidation of carbon monoxide, decomposition of soot and NO_x in diesel exhausts, Fischer-Tropsch synthesis of hydrocarbons, water–gas shift reactions, catalytic oxidations of other various organic compounds, and catalytic decomposition of industrial dyes.[3] Most of these applications require the iron oxide nanoparticles to be chemically stable, uniform in size, and well-dispersed in liquid media. The pristine nanoparticles of iron oxides lean to aggregate into large clusters because of anisotropic dipolar attraction in magnetic iron oxide nanostructures and thus lose their specific properties associated with single-domain. To prevent such type of aggregation, various capping agents with relatively high concentrations are often required.[4] At the same time, the presence of large amounts of capping agents in these systems may hamper its catalytic activity, due to the binding of the capping agents to the active surface of nanoparticle.[5] In addition, the reactivity of iron oxide particles has been shown to greatly increase as their dimensions are reduced.[6] However, it is still a big challenge to develop simple and reliable synthetic methods for relatively smaller iron oxide nanoparticle with designed chemical components and controlled morphologies, which strongly affect the properties of iron oxide nanomaterials. Particularly, phase selective synthesis of iron oxide nanoparticle of smaller size is very important, as iron oxide have many phases. Till date, few methods are available in the literature for phase selective iron oxide synthesis. Wan *et al.* shown the controlled synthesis of three of the most common iron oxides α-Fe_2O_3, γ-Fe_2O_3, or Fe_3O_4, from the reaction between $FeCl_3 \cdot 6H_2O$, urea, and tetrabutylammonium bromide (TBAB) in ethylene glycol by altering the calcinations conditions.[7] Woo *et al.* also prepared maghemite (α-Fe_2O_3) and magnetite (Fe_3O_4) nanoparticles from thermal decomposition of $Fe(CO)_5$ in the presence of residual oxygen of the system and by consecutive aeration.[8] Bronstein *et al.* shown the influence of the Fe–oleate complex structure on its thermal properties and decomposition products, *i.e.*, iron oxide nanoparticles, their size, size distribution, and structure.[9] Recently, Jia *et al.* shown a novel approach for synthesizing single crystal α-Fe_2O_3 nanorings, employing a double

Department of Chemical Sciences, Tezpur University, Napaam, Asaam-784028, India. E-mail: spratihar@tezu.ernet.in; spratihar29@gmail.com

† Electronic supplementary information (ESI) available. See DOI: 10.1039/c4ra04214j

anion-assisted hydrothermal method.[10] Along with this, several other types of surfactants, such as cationic, anionic, or nonionic, have been used for the synthesis of various type of iron oxide.[11] On the other hand, templates such as aluminum-oxide, silica, carbon nanotubes, polymer fibers, and egg-shell membranes have also been employed. Along with these template promoted iron oxide synthesis, metal oxalates [$M(C_2O_4)_{x/2}$] (x = valency of the metal) have been also used as precursors for the production of oxidic and metallic powders.[12] The frequent use of metal oxalates can mainly be attributed to the stability of oxalate salts and the thermal decomposition of the oxalate anion, which results in the formation of metal oxides (or metal) and carbon monoxide (or carbon dioxide).[13] Depending upon the decomposition parameters and chemical composition of the starting material, various iron oxide phases, such as maghemite (γ-Fe_2O_3) and hematite (α-Fe_2O_3), can be selectively obtained. Hermanek *et al.* have reported the formation of nanocrystalline magnetite (Fe_3O_4) particles by heating iron oxalate to (more than) 360 °C under exclusion of air and moisture.[14] Whereas, at higher temperatures (T > 400 °C), the coexistence of metallic (α-Fe) and thermodynamically unstable wüstite (FeO) was observed. The decomposition temperature and atmosphere can substantially influence the oxalate-to-oxide transformation chemistry, because the formation of the final product depends on the selective or simultaneous cleavage of M–O and C–O units in metal oxalates.

Despite a large number of reports available on the application of $Fe(C_2O_4)\cdot 2H_2O$ as precursors, for example, in sol–gel method, hydrothermal techniques, a systematic study on the control of reaction chemistry by the judicious choice of chemical additives (oxidizing or reducing agent) is still on search, which motivated us to undertake this work. Herein, we report an efficient green synthesis of orthorhombic iron(oxalate) capped Fe(0) [Fe(ox)–Fe(0)] nonmaterial using sodium borohydride ($NaBH_4$) reduction of iron(II) salt in presence of oxalic acid at room temperature in water. The reported method is a cost-effective chemical route to produced $Fe(C_2O_4)$ capped iron nano particles [hereafter Fe(ox)–Fe(0)] on gram level without high-temperature calcinations. The morphology has been characterized by different physical methods such as FTIR, XRD, FESEM, and TEM. The transformation of Fe(0) to Fe_3O_4 after keeping the Fe(ox)–Fe(0) at room temperature in water for a prolonged time (1–2 days) also produced $Fe(C_2O_4)$ capped Fe_3O_4 magnetic nanomaterial [hereafter Fe(ox)–Fe_3O_4] in gram scale.

On the other hand, the catalyst separation and reuse have been increasingly important goals in the chemical community from economic, safety, and environmental points of view. The strategy of magnetic separation of nanoparticles is more effective than filtration or centrifugation as it prevents loss of the catalyst. Towards this goal, various strategies have been successfully demonstrated the applications of magnetite Fe_3O_4 nanoparticle-immobilized or -supported catalysts.[15] In this respect, Li *et al.* successfully demonstrated the synthesis of various propargylamines from a robust and magnetically recoverable Fe_3O_4 nanoparticle catalyzed three-component coupling of aldehyde, alkyne, and amine.[16] In view of the influence of green chemistry, it is always better to prevent waste rather than to treat or clean up waste after it has been created.[17] Maintaining greenness in synthetic methodology by prevention of waste, avoiding the use of expensive catalyst or auxiliary substances (*e.g.* solvents, additional reagents) is always needed.[18] Towards this, the magnetic [Fe(ox)–Fe_3O_4] material was found to be useful as a magnetically recoverable catalyst for the synthesis of bis(indolyl)methane derivatives in water. The reusability of [Fe(ox)–Fe_3O_4] nanocatalyst was successfully examined eight times with only a very slight loss of catalytic activity. The as-prepared Fe(ox)–Fe_3O_4 nanomaterials also shown an excellent ability as a recyclable catalyst for the degradation of methylene blue (MB) under UV irradiation in water.

Results and discussions

Characterization of iron nanomaterial

Previous literature showed that $Fe(C_2O_4)\cdot 2H_2O$ crystallizes in two allotropic forms, α monoclinic $C2/c$ and β orthorhombic $Cccm$. As an important contribution, Tirado *et al.* showed the synthesis of mesoporous $Fe(C_2O_4)$ by dehydration (calcination) of bulk monoclinic and micellar orthorhombic $Fe(C_2O_4)\cdot 2H_2O$ precursors at 200 °C.[19] They observed that the nanoribbon shaped particle can be preserved even after dehydration. They further applied the material as high-capacity lithium storage materials with improved rate performance. Herein, we report the synthesis of iron(oxalate) capped Fe(0) [Fe(ox)–Fe(0)] nanomaterial from the aqueous phase room temperature reduction of Mohr's salt, $(NH_4)_2SO_4\cdot FeSO_4$ with sodium borohydride ($NaBH_4$) in presence of oxalic acid. After the completion of reaction, [Fe(ox)–Fe(0)] nanomaterial was separated from the reaction mixture by using an external magnet and washed with water, and dried under vacuum at 50–60 °C. The nanomaterial characterization by X-ray diffraction (XRD) confirm the formation of single-phase orthorhombic $Fe(C_2O_4)\cdot 2H_2O$, as the peaks in XRD are in good agreement with reported XRD pattern of $Fe(C_2O_4)\cdot 2H_2O$ (Fig. 1). From the XRD, we believe the presence of Fe(0) in the material as both the peak for Fe(ox) and Fe(0) overlapped each other. Some of the peaks in XRD are well

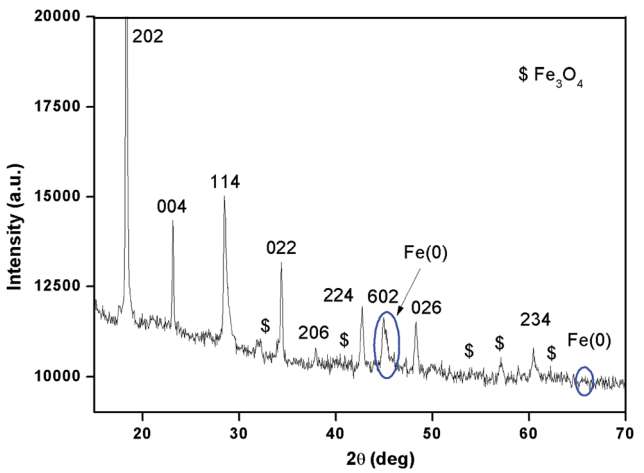

Fig. 1 XRD pattern of Fe(ox)–Fe(0) nano particle.

matched with Fe_3O_4, which further suggests the oxidation of Fe(0) to Fe_3O_4. At this stage, we thought that after sodium borohydride reduction, reduced iron(0) has been trapped in 3-D network of orthorhombic iron oxalate and formed the iron-(oxalate) capped Fe(0) [Fe(ox)–Fe(0)] nanomaterial (Fig. 4). FTIR spectra of oxalic acid, $Fe(C_2O_4)\cdot 2H_2O$, and the synthesized Fe(ox)–Fe(0) nano particle were recorded to know the binding behaviour of oxalic acid in Fe(ox)–Fe(0) nanoparticle. The peak at 1710 cm^{-1} for oxalic acid is characteristic for carbonyl group. Other two peaks for oxalic acid appear at 1260 and 1123, which is due to C–O and C–C bond of oxalic acid (Fig. 2). The characteristic IR bands for *meta* carboxylates are in the range of 1650–1510 cm^{-1} for the asymmetrical vibrations and 1400–1280 cm^{-1} for the symmetrical vibrations. FTIR analysis of $Fe(C_2O_4)\cdot 2H_2O$ shows characteristic peaks at 1640, 1362, 1315, 819, and 493 cm^{-1}. The position and separation of $\nu(COO^-)$ bands, Δ, in the 1300–1700 cm^{-1} region can be used to deduce the carboxylate coordination mode. For $\Delta > 200$ cm^{-1}, a unidentate ligand is expected, whereas for $\Delta < 110$ cm^{-1}, it is a bidentate ligand. For a bridging ligand, Δ remain in between. The peaks at 1640 and 1362 cm^{-1} were typical for metal carboxylate, in which oxalic acid is acting as a bidentate ligand in $Fe(C_2O_4)\cdot 2H_2O$. The other peak at 1315, 819 cm^{-1} occur due to C–O and C–C stretching vibration. The IR band of synthesized Fe(ox)–Fe(0) nanomaterial well matched with $Fe(C_2O_4)\cdot 2H_2O$, which suggest the presence of iron oxalate in the synthesized material. TEM micrographs of Fe(ox)–Fe(0) nanomaterial showed fibrous morphology with layered structure (Fig. 3). Further, the presence of Fe(0) in Fe(ox)–Fe(0) nanomaterial has been checked from the reducing property of the material. For this, reduction reaction of methylene blue was chosen as a model reaction as it can be monitored visually as well as spectrophotometrically.

Determination of iron(0) in oxalate bound iron nanomaterial with reduction of methylene blue

The reversible redox reactions of methylene blue (MB) to leuco methylene blue (LMB) not only provide a delightful reaction, visually dramatic reversible color change, but also provide an engaging with the multifarious illustration of redox phenomena of a species, reaction kinetics, and the principles of chemical titration.[20] There are some reports of reversible MB to LMB redox reactions with the use of various reagents like; sulfite–iodate, iodate–arsenous acid, iodine–bisulfate.[21] Snehalatha *et al.* demonstrates the clock reaction involving methylene blue and L-ascorbic acid.[22] As an important contribution Pande *et al.* showed Cu_2O promoted oscillation between blue MB and colourless LMB solution on periodic shaking.[23] Through various studies they showed that the oscillation cycle between MB and LMB can be reproduced up to endless number due to the formation of redox Cu(II)/Cu(I) system. Using the reversible redox reaction between MB and LMB, we wanted to check the existence of iron(0) nanoparticle in Fe(ox)–Fe(0) nanomaterial. In aqueous medium the initial blue colour of the dye, MB, faded away upon the addition of Fe(ox)–Fe(0) nanomaterial, producing colorless leuco methylene blue (LMB) (Fig. 5). The steady decrease of the two absorbance maxima at two specified band (662 and 290 nm) and appearance of new band at 255 nm due to the formation of leuco methylene blue (LMB) indicates the progress of the reaction (Fig. 5). In the absence of Fe(ox)–Fe(0), no noticeable decrease in absorbance of the dye was observed. The sole use of sodium borohydride ($NaBH_4$) and $Fe(C_2O_4)\cdot 2H_2O$ was also found to be inactive towards the reduction of

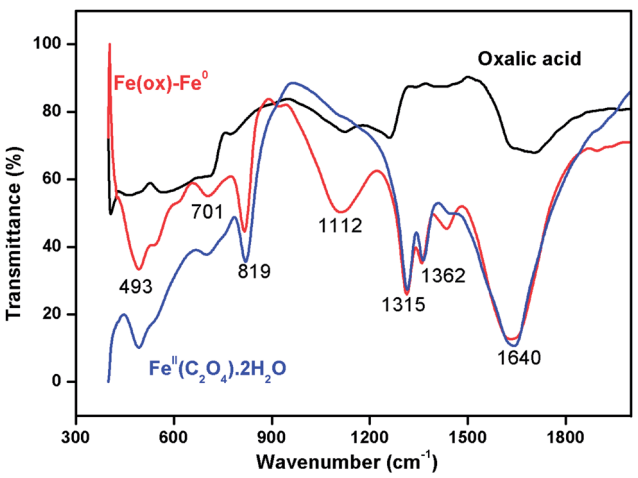

Fig. 2 Comparative FT-IR spectrum of Fe(ox)–Fe(0) with oxalic acid and $Fe(C_2O_4)\cdot 2H_2O$.

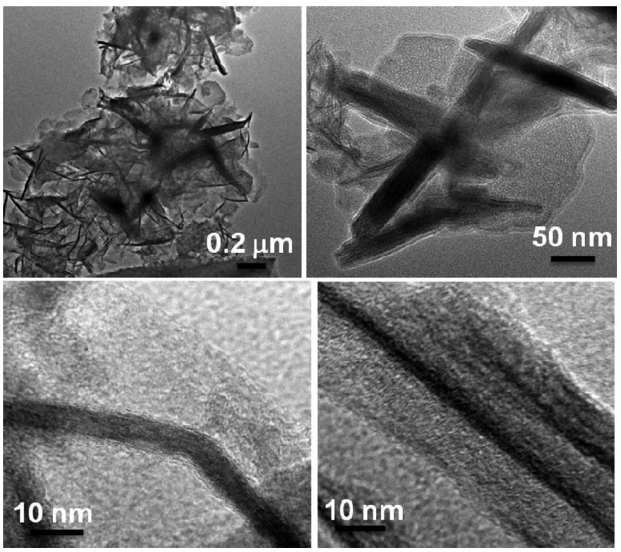

Fig. 3 TEM/HR-TEM image of Fe(ox)–Fe(0).

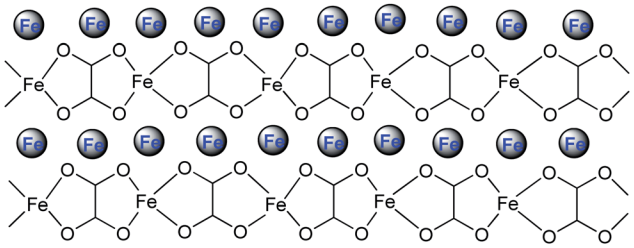

Fig. 4 Schematic diagram of iron oxalate capped iron(0) nanoparticle.

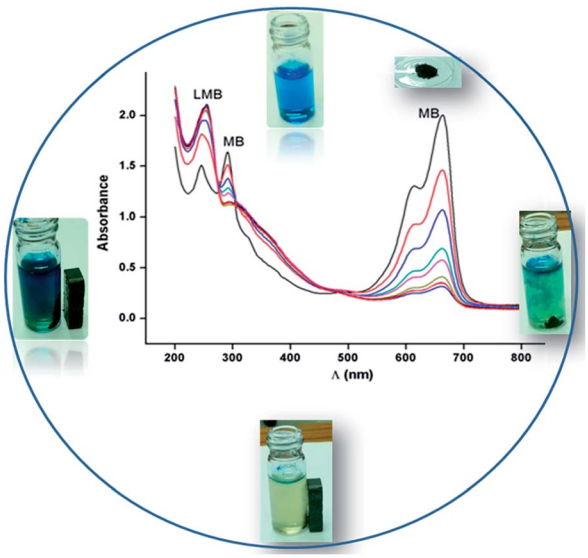

Fig. 5 Fe(ox)–Fe(0) promoted reversible methylene blue to leuco methylene blue redox reaction.

MB to LMB, which further confirms the presence of Fe(0) in Fe(ox)–Fe(0). Interestingly, after the reduction of MB, the observed colourless solution turned into blue, after shaking the colourless reaction mixture or purging air through it at room temperature. While on standing, the blue colour of the solution is diminished again by the addition of excess Fe(ox)–Fe(0) in aqueous solution. The kinetics of Fe(ox)–Fe(0) nanomaterial promoted MB to LMB reduction reaction was done by monitoring the steady decrease of absorbance at 662 nm band at an interval of 5 second. The absorbance *versus* time plot shows a profile of exponential nature, which indicated the pseudo-first-order nature of the reaction (Fig. 6). Furthermore, a plot of ln(*A*) *vs.* time leads to a straight line, further confirms the pseudo-first order reaction kinetics (Fig. 6). The rate constant of iron promoted reduction reaction of MB is 13.3×10^{-3} s^{-1}. Interestingly, freshly prepared Fe(ox)–Fe(0) sample is more active. The activity of the Fe(ox)–Fe(0) material towards the reduction of MB to LMB is decreased upon keeping the sample in open air for prolonged time. This may be due to the lesser no of active Fe(0) particle in Fe(ox)–Fe(0), due to surface oxidation of Fe(0) to Fe_3O_4 in air.

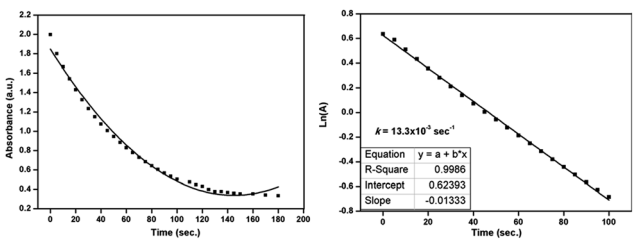

Fig. 6 Rate kinetics of Fe(ox)–Fe(0) catalyzed reduction of methylene blue.

During the course of iron nano particle promoted reduction reaction of MB, black color of iron nanoparticle slowly turned into light brown which may be due to the oxidation of Fe(0) to its oxide. Detailed characterization of the oxide material was done and elaborated in next section.

Iron(0) to iron oxide formation

Preliminary attempts were made to determine the oxidized product of Fe(ox)–Fe(0) nanomaterial by employing UV-vis spectroscopy. The brown material was washed with distilled water and homogeneously dispersed into water to record the absorption behaviour. Interestingly, two absorption peak (Λ_{max} = 307 and 370 nm) was observed in UV-vis window, which corresponds to iron oxide (please see Fig. S1 in ESI†). The FTIR spectrum of brown material showed two peaks at 1415 and 1660 cm^{-1} due to the oxalate coordination to metal oxide (Fig. 7).

The peak at 413 cm^{-1} corresponds to Fe–O symmetric bending vibration and at 563 cm^{-1} corresponds to the Fe–O–Fe. The FT-IR study of the brown material also verifies the presence of oxalate in the oxidized material. Further attempts were made to determine the crystalline phase and degree of crystallinity by employing X-ray diffraction analysis of brown material. The XRD pattern of the sample confirms the structure of Fe_3O_4 nanocrystal because the position and the relative peak intensity of the main peaks are well matched with the JCPDS card (85-1436) for magnetite Fe_3O_4.[8] On the other hand, some of the XRD peak position and intensity also matched with orthorhombic $Fe(C_2O_4)\cdot 2H_2O$. From XRD analysis, we viewed the presence of both Fe(ox) and Fe_3O_4 in the oxidized material [Fe(ox)–Fe_3O_4]. Interestingly, even after keeping the Fe(ox)–Fe(0) sample in open air for 1–2 days also produced brown material at room temperature, which also contained Fe(ox) and Fe_3O_4. So, both the MB oxidation and aerial oxidation of Fe(0) in Fe(ox)–Fe(0) produced brown material, Fe(ox)–Fe_3O_4. A typical TEM image of Fe(ox)–Fe_3O_4 was shown in Fig. 9. The initial fibrous type morphology of Fe(ox)–Fe(0) has been retained in the Fe(ox)–Fe_3O_4, which consists of Fe(ox) template bound Fe_3O_4 nanoparticle.[24] So, aerial oxidation of Fe(0) bound with Fe(ox)

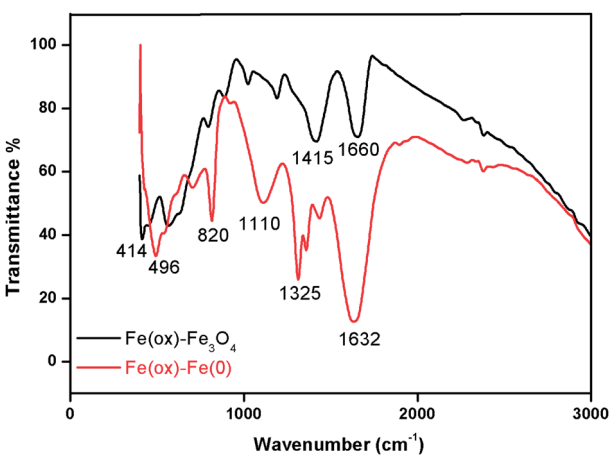

Fig. 7 Comparative FT-IR spectrum of Fe(ox)–Fe(0) and Fe(ox)–Fe_3O_4.

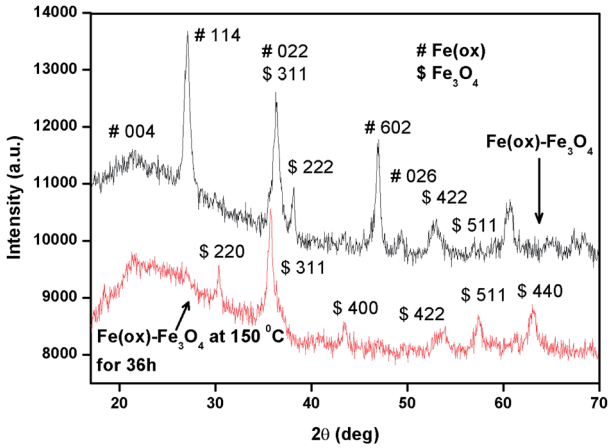

Fig. 8 XRD pattern of Fe(ox)–Fe_3O_4 and its decomposed product Fe_3O_4.

may transform Fe(0) to Fe_3O_4 keeping Fe(ox) intact. The calculated lattice spacing between two planes of Fe(ox)–Fe_3O_4 from HR-TEM was ~0.24 nm (Fig. 9). Further, scanning electron microscope (SEM) of Fe(ox)–Fe_3O_4 material indicates porous layered type structure (Fig. 10). Interestingly, pores are produced between layers as a result of the aggregated assembly between magnetic nanoparticles.

Furthermore, upon heating the Fe(ox)–Fe_3O_4 at 150 °C in oven for 36 h, brown material transformed into reddish-brown. The XRD pattern of reddish-brown material (Fig. 8) agreed well with the standard XRD pattern of magnetite Fe_3O_4 (magnetite, JCPDS 85-1436). The conversion of Fe(ox)–Fe_3O_4 to Fe_3O_4 may be due to the decomposition of Fe-bound oxalate upon heating. TEM images of decomposed Fe_3O_4 material at different magnification revealed that initial fibrous morphology of Fe(ox)–Fe_3O_4 had been transformed into interconnected nanoparticles, because of the removal of organic species in the

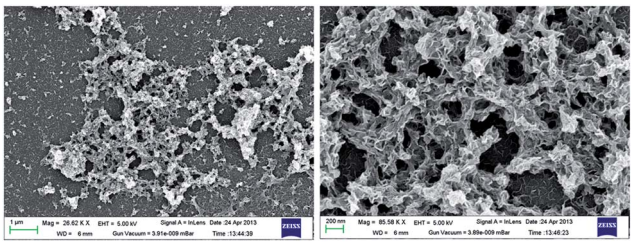

Fig. 10 HR-SEM image of Fe(ox)–Fe_3O_4.

precursor upon heating the Fe(ox)–Fe_3O_4 nanomaterial at 150 °C (Fig. 11). The size of these nanoparticles ranged between 4–15 nm. The selected area electron diffraction (SAED) analysis exhibited the high polycrystalline nature of Fe_3O_4 nanoparticle (Fig. S2 in ESI†). The SAED pattern also suggested the formation of Fe_3O_4. We have also analyzed the lattice fringes of the nanocrystal (Fig. 11), the lattice spacing between two planes is observed to be ~0.29 nm, corresponding to the distance of two (220) planes of Fe_3O_4. The SEM image also suggested the agglomerated structure of Fe_3O_4 because of the magnetic dipole interaction between magnetic Fe_3O_4 nanoparticles. Furthermore, EDAX analysis authenticates the elemental composition of the reddish-brown material, confirming the Fe_3O_4 formation (Fig. 12).

The optical property of Fe(ox)–Fe_3O_4 NPs was investigated by DRS experiment. The band gap of the synthesized material has been calculated from the plot of $(\alpha E_p)^2$ *versus* E_p based on the direct transition and the extrapolated value of E_p at $\alpha = 0$. The band gap value of Fe(ox)–Fe_3O_4 material was found to be 2.0 eV. On the other hand, the band gap value of Fe_3O_4 is 1.7 eV (Fig. S2 and S3 in ESI†). The slightly higher band gap of the Fe(ox)–Fe_3O_4 compared to Fe_3O_4 may be attributed to small particle size and some crystal lattice defects.[25] The catalytic application of

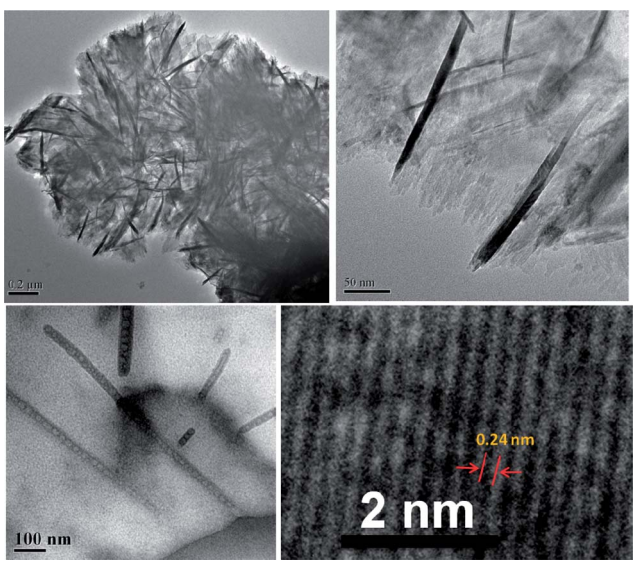

Fig. 9 TEM/HR-TEM image of Fe(ox)–Fe_3O_4.

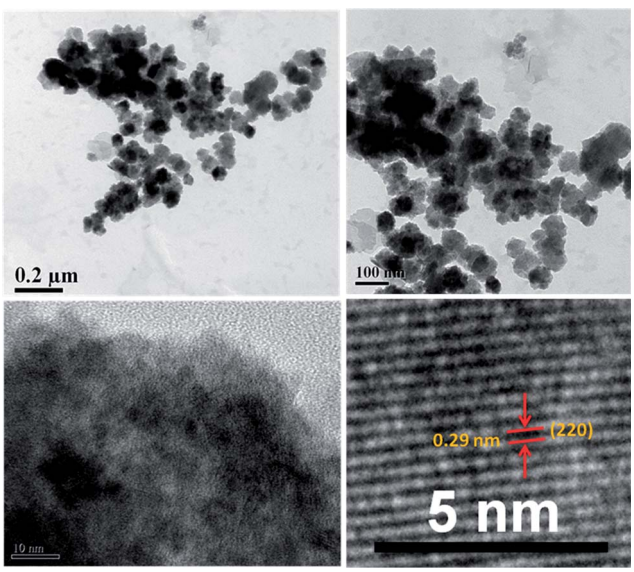

Fig. 11 TEM/HR-TEM image of Fe_3O_4.

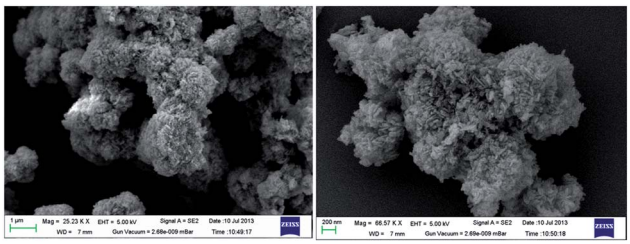

Fig. 12 HR-SEM image of Fe_3O_4.

Fe(ox)–Fe_3O_4 magnetic material towards organic transformation and photo degradation reaction in water has been done and elaborated in next section.

Fe(ox)–Fe_3O_4 promoted synthesis of bis(indolyl) methanes

The development of new methodologies for the synthesis of bis(indolyl)methanes has received considerable amount of interest to synthetic organic/medicinal chemists since bis(indolyl)methanes possess a wide range of biological activity.[26] Generally bis(indolyl)methanes are prepared by the condensation of indoles with various aldehydes or ketones in the presence of catalyst such as; protic or Lewis acids inorganic or organic salt, ionic liquid or ionic liquid in conjugation with some Lewis acids, zeolite, silica supported catalyst, *etc.*[27] However, some of the reported methods have one or more of the following limitations: for example, use of expensive catalyst and volatile organic solvents, tedious work-up, complicated reaction set-up, longer reaction times, low-yields of products, *etc.* In terms of environmental compatibility, reusability, operational simplicity, and ease of isolation, we also wanted to check the activity of Fe(ox)–Fe_3O_4 towards the synthesis of bis(indolyl) methanes. The reaction between 4-bromo benzaldehyde and indole has been chosen as a model reaction for the study. Among the solvents tested, water was the most effective reaction medium for this condensation reaction. Other organic solvent like methanol, ethanol, dimethyl sulfoxide (DMSO) are also effective for the reaction. But, slightly lower yields were obtained with the solvent like dichloroethane, toluene, tetrahydrofuran (THF). When compared to other known catalytic system, we found superiority of Fe(ox)–Fe_3O_4 material towards the condensation between 4-bromo benzaldehyde and indole in water at 100 °C in air (Table 1). The Fe(ox)–Fe_3O_4 nanomaterial catalyzed model reaction failed at room temperature. Although quantitative yield of bis(indolyl)methanes product **1a** was achieved with Fe(ox)–Fe_3O_4 as a catalyst in water however, in most of the cases, solid lump of product in water was observed. So, after the completion of the reaction, water was removed from the reaction mixture by decantation and acetone was added to the reaction vessel to solubilize the product. After that the insoluble catalyst Fe(ox)–Fe_3O_4 in acetone has been recovered from the reaction mixture with the help of a tiny magnet (Fig. 13). No significant difference was observed when slightly increasing the catalyst loading. But upon decreasing the catalyst mol% from 5 to 2, significant fall down in the product yield has been observed. From screening of solvent, temperature, and catalyst loading the optimized reaction conditions were following: 1.0 equiv. of aldehyde, 2.1 equiv. of indole, and 5 mol% of Fe(ox)–Fe_3O_4 nanoparticles as a catalyst in water at 100 °C in air. Furthermore, the blank test with model reaction under optimized reaction condition provided corresponding bis(indolyl)methane with low yield (Table 1).[28] The involvement of Fe(ox)–Fe_3O_4 towards the formation of bis(indolyl)methanes from the condensation between aldehyde and indoles was done from the FTIR experiment.[29,30]

For practical applications of such heterogeneous magnetically recoverable systems, the lifetime of the catalyst and its reusability are very important factors. For this, a set of experiments was done for the condensation between 4-bromo benzaldehyde and indole using Fe(ox)–Fe_3O_4 nanoparticles as a catalyst. After the completion of the first reaction, the catalyst was recovered magnetically, washed with acetone for 3–4 times. A new reaction was then performed with fresh reactants under the optimized reaction conditions.

Table 1 Effect of catalyst for the synthesis of bis(indolyl)methanes in water

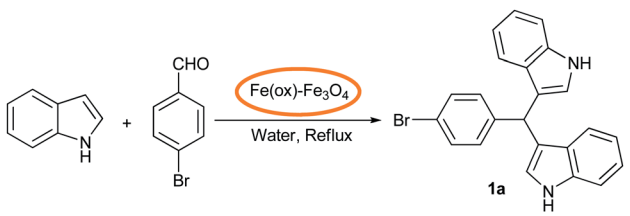

#	Catalyst	Mol (%)	Time (h)	Yield (%)
1	Fe(ox)–Fe_3O_4	10	2	89
2	Fe(ox)–Fe_3O_4	5	2	90
3	Fe(ox)–Fe_3O_4	2	6	68
4	Fe_3O_4	5	6	41
5	$FeCl_3 \cdot 6H_2O$	5	6	17
6	$FeCl_2 \cdot 6H_2O$	5	6	14
7	Oxalic acid	5	6	22
8	Iodine	5	6	12
9	—	—	6	21

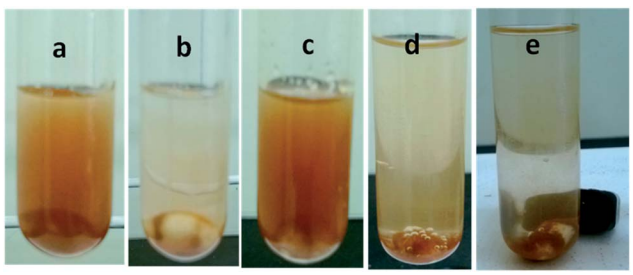

Fig. 13 Photo of (a): Fe(ox)–Fe_3O_4 nanoparticle in water; (b): Fe(ox)–Fe_3O_4 nanoparticle adsorbed on the magnetic stirring bar; (c): Fe(ox)–Fe_3O_4 nanoparticle in the reaction mixture; (d): after the completion of reaction in acetone–water; (e): a magnet attract the Fe(ox)–Fe_3O_4 nanoparticle and magnetic stirring bar.

In terms of TOF, Fe(ox)–Fe_3O_4 catalyst could be reused at least 5 times without any change in activity (Fig. 14). However, slight drop down in the product yield and TOF was observed in 6–8th cycle. The XRD analysis of the used Fe(ox)–Fe_3O_4 nanomaterial after 8th cycle was done. No appreciable change was found in the XRD spectrum, which indicates the robustness of the synthesized Fe(ox)–Fe_3O_4 material (Fig. 15). The generality of the reaction has been tested with various aldehydes and indoles under optimized reaction condition (Table 2). The reaction with the electron-withdrawing aldehydes went smoothly. However, the electron-donating group containing aldehyde gave slightly lower yield of the corresponding bis(indolyl)methanes. We have also tried the reaction with electron rich aldehyde such as; 4-(*n*,*n*-dimethyl) benzaldehyde and pentanal. In both the cases, reaction do not proceed to lead any bis(indolyl)methane derivatives. On the other hand, both electron-donating and withdrawing group containing indoles underwent the condensation reaction smoothly to provide the desired bis(indolyl)methanes product in moderate to good yields.

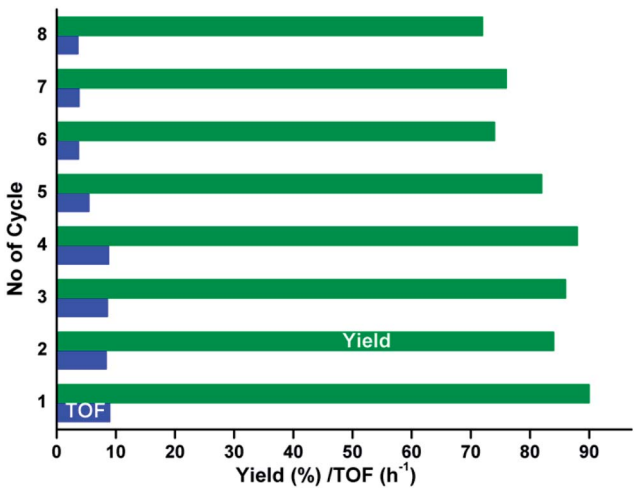

Fig. 14 Catalytic cycle *vs.* turn over frequency (TOF) and yield plot of Fe(ox)–Fe_3O_4 catalyzed condensation reaction between 4-bromo benzaldehyde and indole.

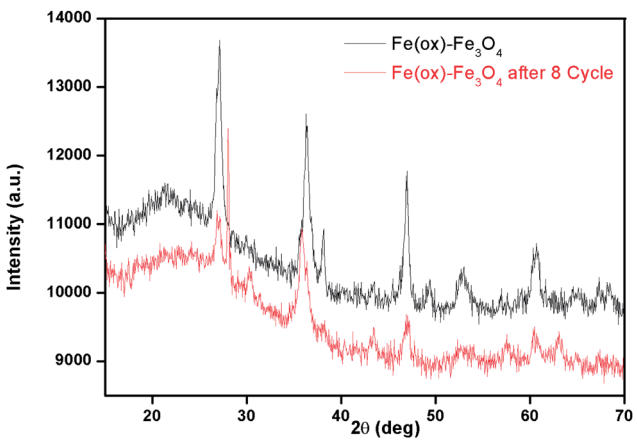

Fig. 15 XRD pattern of Fe(ox)–Fe_3O_4 before and after the completion of 8 cycle.

Table 2 Substrate scope for Fe(ox)–Fe_3O_4 catalyzed condensation reaction between aldehyde and indoles in water

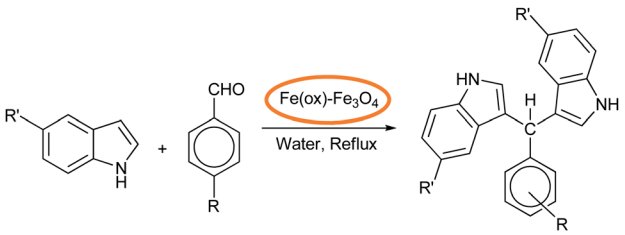

#	R	R′	Product	Time (h)	Yield (%)
1	H	H	**1a**	1	90
2	Me	H	**1b**	2	82
3	Br	H	**1c**	1	90
4	NO_2	H	**1d**	1	92
5	Br	OMe	**1e**	1	78
6	NO_2	NO_2	**1f**	3	76
7	NO_2	Br	**1g**	3	85
8	Me	OMe	**1h**	4	68
9	Me	NO_2	**1i**	4	72
10	H	OMe	**1j**	3	81

Application of Fe(ox)–Fe_3O_4 towards the degradation of methylene blue

The robust metal oxide material catalyzed photo degradation is very important to clean the industrial effluents especially colored dye from textile, paper, pulp, and various industries.[31] The photo degradation of any dye is related to the surface of the oxide material and also to the light source (UV light or visible light). To know the photo catalytic activity of the porous Fe(ox)–Fe_3O_4 material, methylene blue solution was used as a representative dye. The Fe(ox)–Fe_3O_4 photocatalyst (10 mg) was suspended in 5 mL of aqueous solution of MB (2×10^{-5} M). Then, the solution was exposed to UV irradiation (365 nm) at room temperature and time-dependent photo degradation of the dye was studied using UV-vis absorption spectrophotometer. Gratifyingly, magnetically recoverable Fe(ox)–Fe_3O_4 nanomaterial catalyzed degradation of MB was observed in the presence of UV light. The degradation of MB was found to be very slow process in visible light (Fig. 16). However, in absence of Fe(ox)–Fe_3O_4, the photo degradation of MB was stopped. To know the effect of catalyst amount on the photo degradation of MB, the rate kinetics was studied with varying amount of Fe(ox)–Fe_3O_4. There is an enhancement of photo degradation rate of MB with the increase of catalyst concentration up to certain limit. After that, the photo degradation rate is independent with catalyst amount (Fig. 17). The magnetically recoverable Fe(ox)–Fe_3O_4 catalyst could be reused at least 10 times with no appreciable loss in its activity. The adsorption plays very crucial role in the degradation of dye.[32] For this the Fe(ox)–Fe_3O_4 promoted reaction of methylene blue was carried

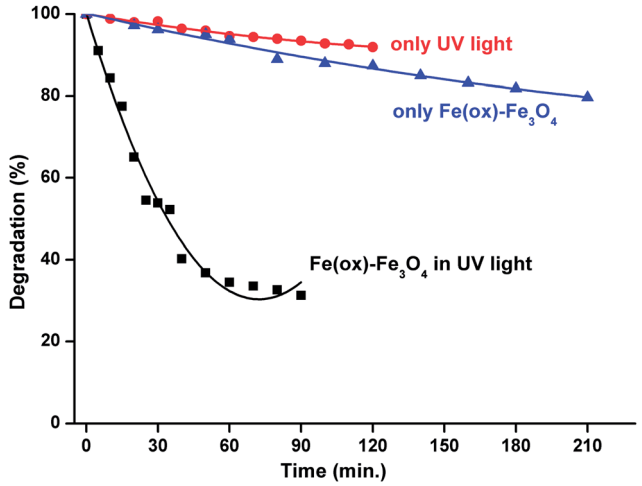

Fig. 16 Fe(ox)–Fe_3O_4 promoted photo degradation of methylene blue under different environment.

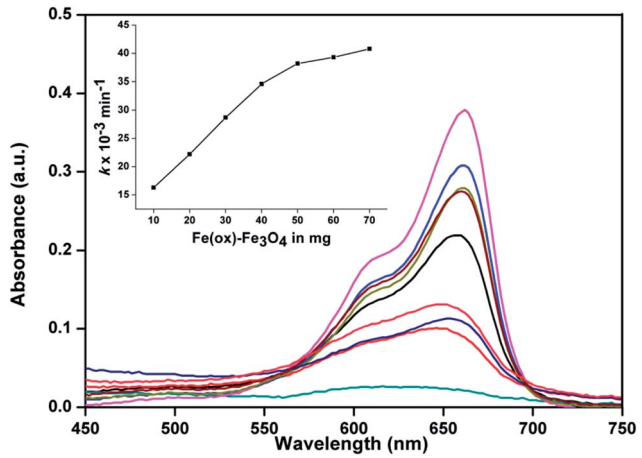

Fig. 17 Fe(ox)–Fe_3O_4 promoted photo degradation of methylene blue under UV-light and the effect of catalyst on photodegradation rate.

out in dark. Interestingly, no gradual hypochromic shift was observed in the dark, but slight decrease in absorbance was found, which suggest slight adsorption of the MB in dark after prolonged time (Fig. S12 and S13†).[33] We have also tried the degradation reaction for other dye like rhodamine B or rose Bengal. Although, the slow degradation rate was found for rhodamine B, but no degradation was observed for rose Bengal.

Experimental section

Synthesis of iron nanoparticle

In a typical procedure, 284 mg of Mohr's salt, $(NH_4)_2SO_4 \cdot FeSO_4$ was taken in 150 mL of distilled water in a 500 mL conical flask. To this 252 mg of oxalic acid, $H_2C_2O_4 \cdot 2H_2O$ was added and stirred vigorously. In another 500 mL conical flask, a solution of 1.2 g of sodium borohydride, $NaBH_4$ was prepared in 100 mL distilled water. Now, $NaBH_4$ solution was added slowly in an earlier prepared solution with vigorous stirring. During the addition, the color of the solution slowly turned to yellow. After few minutes, black Fe nano particle began to appear in a solution, which was separated from the solution with one tiny magnet and washed with water, and dried under vacuum at 50 to 60 °C, and collected for further study.

Reversible redox reaction between MB and LMB

At first a 50 mL of aqueous homogeneous solution of methylene blue (10^{-3} M) was prepared for the study. Then 200 μL of the stock solution has been mixed with 20 mg of Fe(ox)–Fe(0) nanomaterial in a UV-cuvette to record the progress of the reaction. The progress of the reaction has been accounted from a steady decrease of the two absorbance maxima at specified band (662 and 290 nm) positions. At the same time one steady increase of absorbance maxima at specified band of 255 nm was also observed due to the formation of reduced leuco methylene blue (LMB). The blue color of MB disappeared in 2 min. The solution regained its original blue color just after shaking. The visual dramatic reversible color change goes on for about 5 cycles by shaking and resting the reaction mixture with Fe(ox)–Fe(0).

Degradation of methylene blue (MB) with Fe(ox)–Fe_3O_4

At first a 50 mL of aqueous homogeneous solution of methylene blue (10^{-3} M) has been prepared for the study. Then 100 μL of the stock solution has been mixed with 20 mg of Fe(ox)–Fe_3O_4 nanoparticle in a 5 mL conical flask, and the volume of the solution made up to 3 mL and kept under UV-light. The progress of the reaction has been accounted from a steady decrease of the absorbance maxima at specified band (662 nm) positions (Fig. 15).

Typical procedure for Fe(ox)–Fe_3O_4 catalyzed condensation reaction between aldehydes and indoles

In a 10 mL Schlenk flask equipped with a magnetic bar, was charged with Fe(ox)–Fe_3O_4 (0.05 mmol), in water (3 mL) in open air and stirred vigorously for 5 min. After that the appropriate aldehyde (1 mmol) and indole (2.2 mmol) was added to it and placed into a constant temperature bath at 110 °C and allowed to continue. After completion, acetone was added to the reaction mixture to solubilize the product. The catalyst was separated with one tiny magnet and the product extracted with ethylacetate (20 mL × 3) and washed with water (10 mL × 3), brine (10 mL) and dried over anhydrous Na_2SO_4. After removing the solvent the residue was subjected to silica gel column chromatography (60–120 mesh, ethyl acetate–petroleum ether, and gradient elution) to afford pure cross coupling product.

Instruments

Absorption spectra were recorded in a Dynamica Halo DB-30 double beam digital spectrophotometer (Switzerland) attached with a Lab Companion RW-0525G chiller, and also in SHIMADZU UV 2550 spectrophotometer with quartz cuvette. All the samples for FTIR study were properly washed with distilled water at least five times, and then dried under vacuum. Finally, samples for the FTIR spectra were recorded using IMPACT 410

Thermo-Nicolet instrument from a thin transparent KBr pellet. The XRD patterns of the sample was recorded on a Philips PW-1710 X-ray diffractometer (40 kV, 20 mA) using Cu Kα radiation (k = 1.5418 Å) in the 2θ range of 10–90° at a scanning rate of 0.5° min^{-1}. The XRD data were analyzed using JCPDS software. Surface morphology of all the samples were recorded by using a scanning electron microscope (JEOL JSM5800) with an accelerated voltage 5–20 kV. TEM images were acquired using JEOL JEM-2010 microscopes with an operating voltage of 200 kV.

NMR data of bis(indolyl) methanes

1a. δ_H (400 MHz; acetone-d_6) 5.89 (1H, s, –CH), 6.78 (2H, s), 6.86 (2H, t, J = 8.0 Hz), 7.03 (2H, t, J = 8.0 Hz), 7.15 (1H, t, J = 7.6 Hz), 7.24 (2H, t, J = 7.6 Hz), 7.31–7.38 (6H, m), 9.97 (2H, s, –NH). δ_C (100 MHz, Acetone-d_6) 40.3, 111.3, 118.5, 119.0, 119.4, 121.2, 123.7, 125.8, 127.2, 128.0, 128.7, 137.3, 145.1.

1b. δ_H (400 MHz; acetone-d_6): 2.25 (3H, s, –CH_3) 5.83 (1H, s, –CH), 6.76 (2H, s), 6.85 (2H, t, J = 7.6 Hz), 7.00–7.05 (4H, m), 7.24 (2H, d, J = 8.2 Hz), 7.30–7.36 (4H, m), 9.97 (2H, s, –NH). δ_C (100 MHz, acetone-d_6) 28.4, 39.9, 111.3, 118.4, 119.2, 119.5, 121.2, 123.7, 127.3, 128.6, 128.6, 135.0, 137.3, 142.1.

1c. δ_H (400 MHz; DMSO-d_6): 5.79 (1H, s, –CH), 6.79–6.83 (4H, m), 7.00 (2H, t, J = 8.0 Hz), 7.22–7.32 (6H, m), 7.40 (2H, d, J = 8.0 Hz), 10.4 (2H, s, –NH). δ_C (100 MHz, DMSO-d_6) 40.0, 112.0, 118.0, 118.8, 119.3, 119.5, 121.5, 124.1, 127.0, 131.0, 131.4, 137.1, 144.9.

1d. δ_H (400 MHz; acetone-d_6): 6.07 (1H, s, –CH), 6.86–6.91 (4H, m), 7.06 (2H, t, J = 7.2 Hz), 7.32 (2H, d, J = 7.6 Hz), 7.38 (2H, d, J = 7.6 Hz), 7.62 (2H, s), 8.12 (2H, d, J = 8.4 Hz), 10.1 (2H, s, –NH). δ_C (100 MHz, acetone-d_6) 40.1, 111.5, 117.6, 118.8, 119.2, 121.5, 123.3, 124.0, 126.9, 129.7, 137.3, 146.5, 153.1.

1e. δ_H (400 MHz; acetone-d_6): 3.60 (6H, s, –OMe), 5.80 (1H, s, –CH), 6.72 (2H, s), 6.79 (4H, s), 7.24–7.32 (4H, m), 7.41 (2H, d, J = 7.0 Hz), 9.86 (2H, s, –NH). δ_C (100 MHz, acetone-d_6) 39.7, 54.9, 101.5, 111.3, 112.0, 118.0, 119.1, 124.5, 127.5, 130.8, 131.0, 132.4, 144.6, 153.6.

1f. δ_H (400 MHz; acetone-d_6): 6.48 (1H, s, –CH), 7.20 (2H, s), 7.59 (2H, d, J = 9.2 Hz), 7.72 (2H, d, J = 8.8 Hz), 8.0 (2H, d, J = 9.2 Hz), 8.20 (2H, d, J = 8.8 Hz), 8.36 (2H, s), 10.93 (2H, s, –NH). δ_C (100 MHz, acetone-d_6): 39.1, 112.0, 116.2, 117.1, 119.9, 123.7, 126.1, 127.9, 129.7, 140.3, 141.4, 146.9, 151.5.

1g. δ_H (400 MHz; acetone-d_6): 6.12 (1H, s, –CH), 6.93 (2H, s), 7.19 (2H, d, J = 8.8 Hz), 7.37 (2H, d, J = 8.4 Hz), 7.50 (2H, s), 7.64 (2H, d, J = 8.4 Hz), 8.17 (2H, d, J = 8.4 Hz), 10.33 (2H, s, –NH). δ_C (100 MHz, acetone-d_6): 39.5, 111.8, 113.5, 117.1, 121.5, 123.5, 124.3, 125.7, 128.7, 129.6, 135.9, 146.7, 152.2.

1h. δ_H (400 MHz; acetone-d_6): 2.25 (3H, s, –CH_3), 3.59 (6H, s, –OMe), 5.76 (1H, s, –CH), 6.66–6.72 (2H, m), 6.77–6.81 (4H, m), 7.08 (2H, d, J = 7.6 Hz), 7.23–7.25 (4H, m), 9.81 (2H, s, –NH). δ_C (100 MHz, acetone-d_6): 20.0, 39.9, 54.9, 101.8, 111.0, 111.8, 118.8, 124.4, 124.4, 127.7, 128.6, 132.4, 134.9, 142.1, 153.3.

1i. δ_H (400 MHz; acetone-d_6): 2.26 (3H, s, –CH_3), 6.16 (1H, s, –CH), 7.09–7.13 (5H, m), 7.30 (2H, d, J = 8.4 Hz), 7.98 (2H, d, J = 8.8 Hz), 8.33 (2H, s), 10.81 (2H, s, –NH). δ_C (100 MHz, acetone-d_6): 20.1, 39.1, 111.8, 116.4, 116.8, 121.3, 126.3, 127.5, 128.4, 129.1, 135.9, 140.3, 140.6, 141.1.

1j. δ_H (400 MHz; acetone-d_6): 3.62 (6H, s, –OMe), 5.82 (1H, s, –CH), 6.68–6.74 (2H, m), 6.81–6.83 (4H, m), 7.25–7.29 (4H, m), 7.40 (2H, d, J = 8.4 Hz), 9.84 (2H, s, –NH). δ_C (100 MHz, acetone-d_6): 40.4, 54.9, 101.6, 111.1, 111.8, 118.6, 124.4, 125.8, 127.6, 127.9, 128.7, 132.4, 145.1, 153.5.

Conclusions

In summary, iron(oxalate) capped Fe(0) nanoparticle was synthesized using a facile approach. The aerial oxidation of Fe(0) leads to iron(oxalate) capped Fe_3O_4 nano material, which is found to be useful as a magnetically recoverable catalyst for the selective synthesis of bis(indolyl)methanes from the condensation between aldehydes and indoles in water. In terms of environmental compatibility, reusability, operational simplicity, the magnetic iron(oxalate) capped Fe_3O_4 nanoparticles were very simple, effective and economical. The as-prepared Fe(ox)–Fe_3O_4 nanomaterials also shows an excellent ability as a recyclable catalyst for the degradation of methylene blue (MB) under UV irradiation and are expected to be useful in many other applications.

Acknowledgements

Financial support of this work by DST-New Delhi (to SP for INSPIRE research grant) is gratefully acknowledged. SP fondly dedicate this work to Prof. M. K. Chaudhuri on the occasion of his 66th birthday. SP is also thankful to Anu for her constant help and support.

Notes and references

1 (*a*) C. J. Jia and L. Sun, *J. Am. Chem. Soc.*, 2008, **130**, 16968; (*b*) X. Battle and A. Labarta, *J. Phys. D: Appl. Phys.*, 2002, **35**, R15; (*c*) R. H. Kodama, *J. Magn. Magn. Mater.*, 1999, **200**, 359; (*d*) B. D. Cullity, *Introduction to Magnetic Materials*, Addison-Wesley, Reading, MA, 1972.

2 (*a*) S. Wu, Q. He, C. Zhou, X. Qi, X. Huang, Z. Yin, Y. Yang and H. Zhang, *Nanoscale*, 2012, **4**, 2478; (*b*) S. Sun and H. Zeng, *J. Am. Chem. Soc.*, 2002, **124**, 8204; (*c*) A. H. Latham and M. E. Williams, *Acc. Chem. Res.*, 2008, **41**, 411; (*d*) S. Laurent, D. Forge, M. Port, A. Roch, C. Robic, L. V. Elst and R. N. Muller, *Chem. Rev.*, 2008, **108**, 2064.

3 (*a*) V. Polshettiwar, B. Baruwati and R. S. Varma, *Green Chem.*, 2009, **11**, 127; (*b*) A. Hu, G. T. Yee and W. Lin, *J. Am. Chem. Soc.*, 2005, **127**, 12486.

4 (*a*) R. Psaro, A. Fusi, R. Ugo, J. M. Basset, A. K. Smith and F. Hugues, *J. Mol. Catal.*, 1980, **7**, 511; (*b*) M. V. Kovalenko, M. I. Bodnarchuk, R. T. Lechner, G. Hesser, F. Schaffler and W. Heiss, *J. Am. Chem. Soc.*, 2007, **129**, 6352; (*c*) X. W. Teng and H. Yang, *J. Mater. Chem.*, 2004, **14**, 774; (*d*) J. E. Macdonald, C. J. Brooks and J. G. C. Veinot, *Chem. Commun.*, 2008, 3777.

5 M. Hermanek, R. Zboril, I. Medrik, J. Pechousek and C. Gregor, *J. Am. Chem. Soc.*, 2006, **128**, 1675–1682.

6 E. O. Kajander and N. Ciftcioglu, *Proc. Natl. Acad. Sci. U. S. A.*, 1998, **95**, 8274.
7 L.-S. Zhong, J.-S. Hu, H.-P. Liang, A.-M. Cao, W.-G. Song and L.-J. Wan, *Adv. Mater.*, 2006, **18**, 2426.
8 K. Woo, J. Hong, S. Choi, H.-W. Lee, J.-P. Ahn, C. S. Kim and S. W. Lee, *Chem. Mater.*, 2004, **16**, 2814.
9 L. M. Bronstein, X. Huang, J. Retrum, A. Schmucker, M. Pink, B. D. Stein and B. Dragnea, *Chem. Mater.*, 2007, **19**, 3624.
10 C. J. Jia, L. D. Sun, F. Luo, X. D. Han, L. J. Heyderman, Z. G. Yan, C. H. Yan, K. Zheng, Z. Zhang, M. Takano, *et al.*, *J. Am. Chem. Soc.*, 2008, **130**, 16968.
11 C. Cavelius, K. Moh and S. Mathur, *Cryst. Growth Des.*, 2012, **12**, 5948.
12 (*a*) W. Wendlandt, *Anal. Chem.*, 1958, **30**, 58; (*b*) J. M. Heintz and J. C. Bernier, *J. Mater. Sci.*, 1986, **21**, 1569; (*c*) P. K. Dutta, P. K. Gallagher and J. Twu, *Chem. Mater.*, 1993, **5**, 1739; (*d*) C. Drouet and P. Alphonse, *J. Mater. Chem.*, 2002, **12**, 3058.
13 (*a*) A. K. Vijh, *J. Mater. Sci. Lett.*, 1988, **7**, 513; (*b*) D. Dollimore, *Thermochim. Acta*, 1987, **117**, 331.
14 M. Hermanek, R. Zboril, M. Mashlan and L. MacHala, *J. Mater. Chem.*, 2006, **16**, 1273.
15 (*a*) M. Shokouhimehr, Y. Piao, J. Kim, Y. Jang and T. Hyeon, *Angew. Chem., Int. Ed.*, 2007, **46**, 7039; (*b*) M. Shokouhimehr, J. E. Lee, S. I. Han and T. Hyeon, *Chem. Commun.*, 2013, **49**, 4779; (*c*) L. Xu and J. Wang, *Environ. Sci. Technol.*, 2012, **46**, 10145; (*d*) R. Dey, N. Mukherjee, S. Ahammed and B. C. Ranu, *Chem. Commun.*, 2012, **48**, 7982; (*e*) R. Hudson, C.-J. Li and A. Moores, *Green Chem.*, 2012, **14**, 622; (*f*) R. Luque, B. Baruwati and R. S. Varma, *Green Chem.*, 2010, **12**, 1540; (*g*) R. K. Sharma, Y. Monga, A. Puri and G. Gaba, *Green Chem.*, 2013, **15**, 2800.
16 T. Zeng, W.-W. Chen, C. M. Cirtiu, A. Moores, G. Song and C.-J. Li, *Green Chem.*, 2010, **12**, 570.
17 (*a*) P. T. Anastas and J. C. Warner, *Green Chemistry: Theory and Practice*, Oxford University, Oxford, 1998; (*b*) K. Alfonso, J. Colberg, P. J. Dunn, T. Fevig, S. Jenings, T. A. Johnson, H. P. Klein, C. Knight, M. A. Nagy, D. A. Perry and M. Stefaniak, *Green Chem.*, 2008, **10**, 31; (*c*) C.-J. Li and P. T. Anastas, *Chem. Soc. Rev.*, 2012, **41**, 1413.
18 (*a*) D. Guin, B. Baruwati and S. V. Manorama, *Org. Lett.*, 2007, **9**, 1419; (*b*) B. Kaboudin, R. Mostafalua and T. Yokomatsu, *Green Chem.*, 2013, **15**, 2266; (*c*) J. H. Clark, *Green Chem.*, 1999, **1**, 1; (*d*) A. R. Sheldon, *Green Chem.*, 2005, **7**, 267; (*e*) C. E. Song and S. G. Lee, *Chem. Rev.*, 2002, **102**, 3495.
19 M. J. Aragon, B. Leon, C. P. Vicente and J. L. Tirado, *Inorg. Chem.*, 2008, **47**, 10366.
20 H. Landolt, *Ber. Dtsch. Chem. Ges.*, 1886, **19**, 1317.
21 (*a*) E. Mambo and R. H. Simoyi, *J. Phys. Chem.*, 1993, **97**, 13662; (*b*) G. Lente and I. Fabian, *Inorg. Chem.*, 2004, **43**, 4019; (*c*) A. P. Oliveira and R. B. Faria, *J. Am. Chem. Soc.*, 2005, **127**, 18022.
22 T. Snehalatha, K. C. Rajanna and P. K. Saiprakash, *J. Chem. Educ.*, 1997, **74**, 228.
23 S. Pande, S. Jana, S. Basu, A. K. Sinha, A. Datta and T. Pal, *J. Phys. Chem. C*, 2008, **112**, 3619.
24 Although from TEM, SEM, XRD, and reducing behavior towards methylene blue reduction, we have proposed the morphology and characteristics of the material. But, to know inherent connection between Fe(ox)–Fe(0) and Fe(ox)–Fe_3O_4, further study is required.
25 (*a*) H. Zhang, Z. Ji, T. Xia, H. Meng, C. Low-Kam, R. Liu, S. Pokhrel, S. Lin, X. Wang, Y.-P. Liao, M. Wang, L. Li, R. Rallo, R. Damoiseaux, D. Telesca, L. Madler, Y. Cohen, J. I. Zink and A. E. Nel, *ACS Nano*, 2012, **6**, 4349; (*b*) H. El Ghandoor, H. M. Zidan, M. M. H. Khalil and M. I. M. Ismail, *Int. J. Electrochem. Sci.*, 2012, **7**, 5734; (*c*) A. K. Sinha, M. Pradhan, S. Sarkar and T. Pal, *Environ. Sci. Technol.*, 2013, **47**, 2339.
26 (*a*) P. Diana, A. Carbone, P. Baraja, A. Montalbano, A. Martorana, G. Dattolo, O. Gia, L. D. Via and G. Cirrincione, *Bioorg. Med. Chem. Lett.*, 2007, **17**, 2342; (*b*) A. S. Kalgutkar, B. C. Crews, S. W. Rowlinson, A. B. Marnett, K. R. Kozak, R. P. Remmel and L. J. Marnett, *Proc. Natl. Acad. Sci. U. S. A.*, 2000, **97**, 925; (*c*) H.-C. Zhang, L. V. R. Bonaga, H. Ye, C. K. Derian, B. P. Damiano and B. E. Maryanoff, *Bioorg. Med. Chem. Lett.*, 2007, **17**, 2863; (*d*) R. J. Sundberg, *The Chemistry of Indoles*, Academic Press, New York, 1996; (*e*) A. Casapullo, G. Bifulco, I. Bruno and R. Riccio, *J. Nat. Prod.*, 2000, **63**, 447.
27 (*a*) A. K. Chakraborti, S. R. Roy, D. Kumar and P. Chopra, *Green Chem.*, 2008, **10**, 1111; (*b*) M. Roomi and S. MacDonald, *Can. J. Chem.*, 1970, **48**, 139142; (*c*) R. Nagarajan and P. T. Perumal, *Tetrahedron*, 2002, **58**, 1229; (*d*) J. S. Yadav, B. V. Subba Reddy, C. V. S. R. Murthy, G. M. Kumar and C. Madan, *Synthesis*, 2001, **5**, 783; (*e*) S.-J. Ji, M.-F. Zhou, D.-G. Gu, S.-Y. Wang and T.-P. Loh, *Synlett*, 2003, 2077; (*f*) S.-J. Ji, M.-F. Zhou, D.-G. Gu, Z.-Q. Jiang and T.-P. Loh, *Eur. J. Org. Chem.*, 2004, 1584; (*g*) S.-J. Ji, S.-Y. Wang, Y. Zhanga and T.-P. Loh, *Tetrahedron*, 2004, **60**, 2051.
28 We have also performed blank test with different aldehydes and indoles in water. But, in most of the cases, very low yield of the corresponding bis(indolyl)methanes was observed in the absence of Fe(ox)–Fe_3O_4 catalyst (please see Table S1 in ESI†).
29 The FTIR spectrum of 4-bromo benzaldehyde (**2a**) shows two peaks at 1693 and 1577 cm^{-1} due the stretching vibration of C=O. The peaks at 2763 and 2855 cm^{-1} are due to C–H stretching vibration of **2a**. To know the involvement of the catalyst in the reaction, 1 : 1 mixture of Fe(ox)–Fe_3O_4 and **2a** was taken in a motor pestle and grinded for 0.5 h. The FTIR analysis of the mixture showed shifting of peaks for both the C=O and C–H stretching vibration to lower wave numbers as compared to free aldehyde. The possible shift to lower wave number is evident for the intimate interaction between Fe(ox)–Fe_3O_4 catalyst and carbonyl group (for details please see ESI†).
30 (*a*) A. Stolle, T. Gallert, C. Schmöger and B. Ondruschka, *RSC Adv.*, 2013, **3**, 2112 and references therein; (*b*) T. J. LuPage and K. B. Wiberg, *J. Am. Chem. Soc.*, 1988, **110**, 6643.

31 (*a*) A. L. Linsebigler, G. Lu and J. T. Yates, *Chem. Rev.*, 1995, **95**, 735; (*b*) A. K. Sinha, M. Basu, M. Pradhan, S. Sarkar, Y. Negishi and T. Pal, *J. Phys. Chem. C*, 2010, **114**, 21173; (*c*) R. Abe, H. Takami, N. Murakami and B. Ohtani, *J. Am. Chem. Soc.*, 2008, **130**, 7780.

32 (*a*) S. R. Segal and S. L. Suib, *Chem. Mater.*, 1997, **9**, 2526; (*b*) Q. Luo, X. Li, Q. Cai, Q. Yan and Z. Pan, *Int. J. Miner., Metall. Mater.*, 2012, **19**, 1045.

33 We thank one of the esteemed reviewers for pointing out this.